Structure of star-burst dendrimers: A comparison between small angle x-ray scattering and computer simulation results

Silke Rathgeber[a)]
Forschungszentrum Jülich GmbH, Soft Matter Department, 52425 Jülich, Germany

Tadeusz Pakula[b)]
Max-Planck-Institute for Polymer Research, 55128 Mainz, Germany and Department of Molecular Physics, Polytechnic of Lodz, Poland

Volker Urban[c)]
European Synchrotron Radiation Facility (ESRF), 38043 Grenoble, France

(Received 30 April 2004; accepted 12 May 2004)

We investigated the generation dependent shape and internal structure of star-burst dendrimers under good solvent conditions using small angle x-ray scattering and molecular modeling. Measurements have been performed on poly(amidoamine) dendrimers with generations ranging from $g=0$ up to $g=8$ at low concentrations in methanol. We described the static form factor $P(q)$ by a model taking into account the compact, globular shape as well as the loose, polymeric character of dendrimers. Monomer distributions within dendrimers are of special interest for potential applications and have been characterized by the pair correlation function $\gamma(r)$, as well as by the monomer and end-group density profile, $\rho(r)$ and $\rho_e(r)$, respectively. Monomer density profiles and $\gamma(r)$ can be derived from $P(q)$ by modeling and via a model independent approach using the inverse Fourier transformation algorithm first introduced by Glatter. Experimental results are compared with computer simulations performed for single dendrimers of various generations using the cooperative motion algorithm. The simulation gives direct access to $\gamma(r)$ and $\rho(r)$, allows an independent determination of $P(q)$, and yields in addition to the scattering experiment information about the distribution of the end groups. Excellent qualitative agreement between experiment and simulation has been found. © *2004 American Institute of Physics.* [DOI: 10.1063/1.1768516]

I. INTRODUCTION

Starburst dendrimers are highly branched polymers with a regular, treelike architecture as sketched in Fig. 1. In a stepwise synthesis multifunctional monomers are added to a multifunctional core. Each synthetic step defines a new generation and leads to a multiplication (× functionality of branching unit) of the number of monomers and terminal groups in the dendrimer.

The heuristic sketch drawn in Fig. 1 implies not only a well-defined globular shape it also suggests that most of the terminal units can be found on the dendrimer surface leading to a congestion of monomers in the outer shell and a decreased monomer density in the core region. This heuristic image has led to a controversial discussion about the morphology of dendrimers since potential applications (Ref. 1 and references therein) of these systems are highly dependent on their structural peculiarities.

For example: (1) an uniform size and shape is required if self-assembling properties of dendrimers are employed for surface modification or manipulation. (2) A large number of modifiable reactive end groups at the surface should lead to multifunctional systems, useful for the design of new catalysts or applications in biomedicine, such as gene transfection, magnetic resonance imaging, and virus inhibition. (3) Cavities in the dendrimer interior are beneficial for their use as host-guest systems for controlled drug delivery or the stabilization of dyes and pigments. However, these structural properties of dendrimers are still discussed controversially.

Scattering experiments[2–12] and computer simulation[13–29] can give valuable information about the shape and internal structure of dendrimers in terms of radial density distributions and the overall dimension of dendrimers. Both methods approach the problem from different directions. Scattering experiments on dilute polymer solutions measure the form factor $P(q)$ of a (single) dendrimer. By modeling or via inverse Fourier transformation (IFT) and subsequent square root deconvolution (SQDEC), the pair correlation function $\gamma(r)$ and the segment density profile $\rho(r)$ can be derived, where r is the radial distance from the center of mass. Despite the assumption of spherical symmetry for the SQDEC, the IFT and SQDEC approach are model independent. Computer simulation experiments intrinsically determine the segment density profile and pair correlation function, leading to $P(q)$ by Fourier transformation. Once good agreement between simulation and scattering experiment is found, from the simulation, in addition to the scattering experiment, reliable information about the distribution of the chain ends in

[a)]Author to whom correspondence should be addressed. Electronic mail: s.rathgeber@fz-juelich.de
[b)]Author to whom correspondence should be addressed. Electronic mail: pakula@mpip-mainz.mpg.de
[c)]Present address: Oak Ridge National Laboratory (ORNL), Oak Ridge, TN 37831.

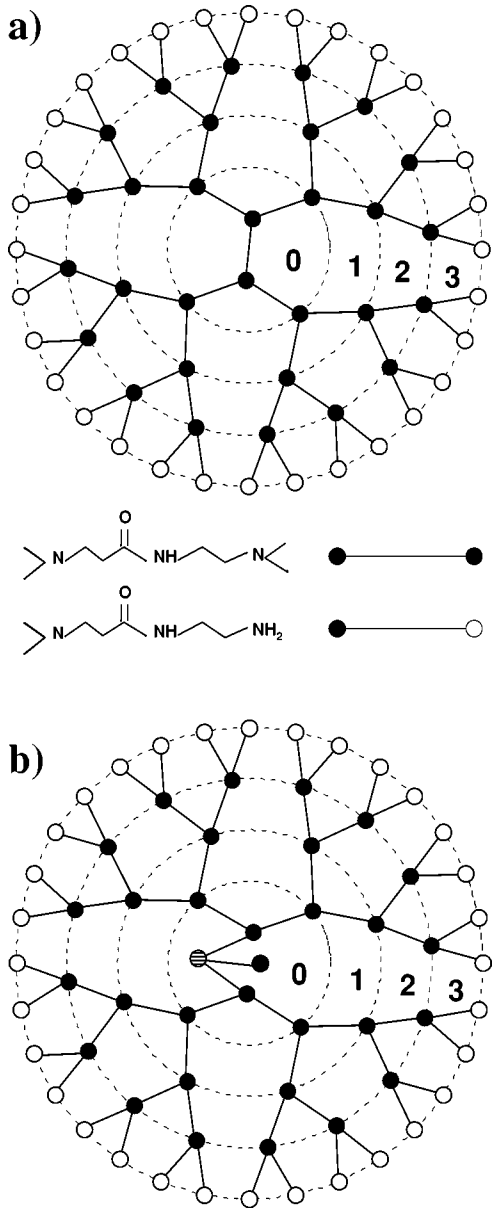

FIG. 1. Schematic representation of third generation dendrimers: (a) a Starburst® poly(amidoamine) (PAMAM) dendrimer and (b) the simulated dendrimer structure. Note, here the counting of the generation starts with $g=0$ which denotes the star polymer.

terms of the end-groups density distribution $\rho_e(r)$ can be obtained. Both methods, experiment and simulation, derive the radius of gyration directly from the pair correlation function.

With this paper we would like to focus on a direct comparison of results obtained from scattering experiments and computer simulation on dendrimers under good solvent conditions.

Our main goal is the detailed discussion of the structural changes occurring in dendrimers as the generation is increased from $g=0$ to 8. We represent the simulated and experimental data in a way enabling a direct comparison in respect to length scales, q-range, and intensities without any adjustable parameters.

The outline of this paper is as follows: In Sec. II we introduce the structural characteristics of the simulated dendrimers as well as those of the poly(amidoamine) (PAMAM) dendrimers. We describe the experimental settings of the scattering experiment and the fundamental concept of the simulation algorithm employed. We explain the basic idea of the model used to describe the scattering spectra and give for both methods an overview over the most important equations necessary to discuss the dendrimer morphology. In Sec. III the results of the simulation and the scattering experiment are summarized with the focus on such quantities which can be determined by scattering and simulation studies. These include (a) the form factor, (b) the segment density profile, (c) the end-group distribution, (d) the molecular weight dependence of the dendrimer dimension and, last but not least, (e) the pair correlation function.

Results are discussed by comparing both methods directly with the focus on the generation dependent changes occurring in the dendritic structure. Section IV contains the most important conclusions.

II. SYSTEMS AND METHODS

A. Samples

The Starburst® poly(amidoamine) (PAMAM) dendrimers were purchased from Dendritech, Inc. in methanol solution. They are synthesized via reiterative reaction sequences starting from a ethylenediamine (EDA) core with functionality $f=4$. Using protection/deprotection strategies a new sequence (generation) can be added, consisting of amine-amide branching units with functionality $m=2$ and spacer length $P=1$. Generation $g=0$ is built up by five segments which include an EDA core molecule plus four amine-amide branching units. The final generation terminates with primary amine end groups. Dendrimers of generation $g=0$ up to $g=8$ were studied. For more detailed information, see Ref. 30. The structural parameters are summarized in Table I and the chemical structure is sketched in Fig. 1(a).

B. Small angle x-ray scattering

The small angle x-ray scattering (SAXS) experiments were performed at the High Brilliance Beamline ID2 at the European Synchrotron Radiation Facility (ESRF) in Grenoble, France. At a wavelength of $\lambda_0=0.1\,\mathrm{nm}$ with a bandwidth of $\Delta\lambda/\lambda_0=2\times10^{-4}$ the evaluated range of scattering vectors was $0.08\,\mathrm{nm}^{-1}<q<3.5\,\mathrm{nm}^{-1}$ using two detector distances $d=10$ and 2 m. As sample containers we used quartz capillaries with a diameter of 1.5 mm. The data were corrected for absorption, background, and detector sensitivity. Experimental q-resolution effects,

$$\Delta q_{\mathrm{FWHM}}=\sqrt{(q\times\Delta\lambda/\lambda_0)^2+(\Delta\theta\times 2\pi/\lambda_0)^2}, \tag{1}$$

where the angular resolution $\Delta\theta$ equals 500 and 100 μrad for $d=2$ and 10 m, respectively, are even so small considered in the data evaluation.

We analyzed the SAXS data via a *model-independent approach* as well as by *direct modeling*. Both approaches and their application to scattering data obtained for PAMAM dendrimers have been described in a previous publication,[10]

TABLE I. Radii of gyration R_g, number of end groups N_e, and total number of segments N for the simulated dendrimer structures initiated from a bifunctional core compared to those of the Starburst® PAMAM dendrimers built from a tetrafunctional core for generations $g=0-8$. The center-to-end-bead distance R_e obtained for the simulated dendrimers and the normalized values $R_g/R_g(g=8)$ are also included.

		Simulation				PAMAM		
g	N_e	N	$R_g/[a]$[b]	$R_g/R_g(g=8)$	R_e	N	R_g[a]/[nm]	$R_g/R_g(g=8)$
0	4	8	1.092 31	0.189	1.464 44	5	0.40 ±0.03	0.104±0.006
1	8	16	1.493 68	0.259	1.960 67	13	0.79 ±0.01	0.204±0.004
2	16	32	1.927 13	0.334	2.377 13	29	1.18 ±0.02	0.306±0.004
3	32	64	2.406 53	0.417	2.801 46	61	1.509±0.005	0.391±0.002
4	64	128	2.9417	0.510	3.309 02	125	1.860±0.007	0.482±0.002
5	128	256	3.557 82	0.617	3.8346	253	2.307±0.003	0.598±0.003
6	256	512	4.249 82	0.737	4.502 43	509	2.750±0.003	0.713±0.002
7	512	1024	4.960 93	0.860	5.203 55	1021	3.211±0.005	0.832±0.002
8	1024	2048	5.768 99	1	5.987 26	2045	3.858±0.01	1.000±0.004

[a]Obtained by IFT and a Gunier fit ($g\leqslant 2$), respectively.
[b]$[a]$ is half of the fcc lattice constant.

therefore here, only a brief overview over the most important equations is given.

The model-independent evaluation derives the pair distance distribution function $p(r)$, or, analogously, the pair correlation function $\gamma(r)=p(r)/r^2$ from the measured scattering intensity via an IFT first introduced by Glatter[31]

$$I(q)=4\pi\int_0^\infty p(r)\frac{\sin(qr)}{qr}dr, \tag{2}$$

from which the radius of gyration

$$R_g^2=\frac{\int_0^\infty p(r)r^2dr}{2\int_0^\infty p(r)dr} \tag{3}$$

can be obtained. Here r is the radial distance from the center of mass. In a second step $p(r)$ yields, under the assumption of spherical symmetry via a square-root deconvolution routine (SQDEC), first introduced by Glatter,[32] the electron density distribution $\rho(r)$

$$p(r)=r^2\int_{-\infty}^\infty \rho(x)\rho(x-r)dx. \tag{4}$$

In particular we used the IFT and SQDEC routines developed by Pederson which are described in detail in Ref. 33.

The maximal dimension $D_{\max}$ and the minimal length scale Δr

$$D_{\max}=\frac{\pi}{q_{\min}} \quad \text{and} \quad \Delta r=\frac{\pi}{q_{\max}}, \tag{5}$$

which can be resolved in real space by this method are determined by the smallest and largest q vector measured in the scattering experiment, $q_{\min}=0.08\,\mathrm{nm}^{-1}$ and $q_{\max}=3.5\,\mathrm{nm}^{-1}$, respectively, yielding $D_{\max}=39\,\mathrm{nm}$ which is about four times larger than the dimension of the $g=8$ dendrimer and $\Delta r=0.9\,\mathrm{nm}$. The value of Δr obtained by Eq. (5) underestimates the lower resolution limit. Extensive tests of Pedersen and Schurtenberger[33] indicate that the resolution is better estimated by $\Delta r\approx 1/q_{\max}$ resulting in a resolution of about 0.3 nm in our particular case. The step width used in Fig. 4 for the representation of the density profiles obtained by IFT and SQDEC has been kept fixed to this value.

The model formulated to describe the scattering data takes into account the loose, polymeric character of dendrimers on small length scales as well their overall compact shape on larger length scales and has been successfully applied in modified versions to other dense polymer systems such as star polymers,[34–37] diblock-copolymer micelles,[38,39] and starlike dendrimers.[40] The dendrimer form factor $P(q)$ can be described by the sum of two contributions

$$P(q)=P_{\text{shape}}(q)+a_bP_{\text{fluc}}(q), \tag{6}$$

where a_b gives the weight of the scattering contribution $P_{\text{fluc}}(q)$ of the internal density fluctuations relative to the scattering contribution $P_{\text{shape}}(q)$ arising from the overall shape of the dendrimers. The latter is derived by modeling the dendrimer density profile by a convolution of a homogeneous sphere profile with radius R_s and a Gaussian distribution with standard deviation σ_s. Depending on the ratio σ_s/R_s, a density profile with a more or less extended plateau in the center region and a smoothly decaying density in a smeared shell region is obtained (see insert of Fig. 5 in Ref. 10 and Fig. 4). Since the Fourier transformation of a convolution simply splits into the product of the Fourier transform of the multipliers, the scattering amplitude $A_{\text{shape}}(q)$ can be expressed in terms of $q_s=qR_s$

$$A_{\text{shape}}(q)=\int_0^\infty \rho(r)r^2\frac{\sin(qr)}{qr}dr=\frac{3}{q_s^3}[\sin(q_s)-q_s\cos(q_s)]\exp\left(-\frac{q^2\sigma_s^2}{4}\right), \tag{7}$$

yielding the shape contribution to the form factor: $P_{\text{shape}}(q)=A_{\text{shape}}^2(q)$.

The internal density fluctuations dominate the scattering at large scattering vectors. On length scales smaller than the correlation length ξ of the density fluctuations, sections of the dendrons have to be described as self-avoiding (sub) walks similar to the case of linear polymers in semiconcentrated solutions. Combining the approaches of Dozier *et al.*[37] and Beaucage,[41] the scattering contribution of the density fluctuations can be described by

$$P_{\text{fluc}}(q) = \frac{1}{\mu q_f^*} \frac{\sin[\mu \tan^{-1}(q_f^*)]}{[1+q_f^*]^{\mu/2}}, \quad \text{with}$$

$$q_f^* = q\xi[\text{erf}(qR_g/\sqrt{6})]^{-3}, \tag{8}$$

where $\mu = \nu^{-1} - 1$ is given by the Flory parameter ν (=3/5 for good solvent conditions). The error function in q_f^* ensures a cutoff of the internal contribution on length scales of the overall dendrimer dimension given by the dendrimer radius of gyration R_g.

The model includes four adjustable parameters: (1) the sphere radius R_s, (2) the width of the smeared surface region determined by the standard deviation σ_s of the Gaussian, (3) the correlation length of the density fluctuations $\xi = 1.5 \pm 0.1$ nm which is found to be independent, Ref. 10 gives a detailed description of the fitting procedure as well as a summary of the fit results in Table I.

C. Computer simulation

Computer simulation of model systems of single dendrimers with generations between $g = 0$ and $g = 8$ have been performed using the cooperative motion algorithm (CMA), in a version previously used for simulations of other single macromolecules with various architectures.[42–44] This method has an unique property of providing sufficient mobility in dense lattice macromolecular systems (all lattice sites occupied) due to the applied concepts of cooperative molecular rearrangements.[42,44–46] It seems to be particularly suitable for simulations of compact macromolecules such as dendrimers or multiarm stars since in such structures the intramolecular density can reach values comparable to the density in bulk. The method has been described in various former publications,[42–46] therefore here, only details related directly to the considered architectures will be given.

Generally, in this type of simulation the macromolecules are considered on a fcc lattice as assemblies of beads, representing monomers, connected by nonbreakable bonds in a way corresponding to the macromolecular skeleton. The particular scheme depicting the polymer skeleton of the simulated dendrimers is shown in Fig. 1(b). The systems represent single molecules which are considered in an open space, i.e., without external boundaries.

Dendrimers of various generations are obtained in a way corresponding to the synthetic routes used in real systems. Starting from a primary initiator of a given functionality, larger regular structures (higher generations) were grown sequentially by extending the reactive ends by linear or branched units according to the requirements given by the assumed structural parameters (e.g., spacer length or branching functionality) and the available space. The simulated dendrimers are flexible and rearrange under the excluded volume condition as if they are immersed in a neutral (good) solvent. During the growth process the structures were kept in motion giving nearly spatially relaxed structures immediately.

Dynamics has been analyzed by means of various correlation functions describing orientational relaxations and displacements. Systems of different generations have been monitored over time periods exceeding the longest relaxation time by at least one order of magnitude in order to be sure that equilibrium has been reached. Simulated dendrimers considered in this paper under athermal conditions are constructed in the following manner: core functionality $f = 4$, length of the spacer between the branching points $P = 1$, branching functionality $m = 2$, and generations from $g = 0$ to 8. Generation $g = 0$ consists of eight beads. Table I summarizes the structural parameters and Fig. 1(b) gives a sketch of the simulated structures by means of the $g = 3$ dendrimer. Figure 2 shows a series of snapshots of equilibrated simulations for dendrimers with generations between $g = 3$ and 7.

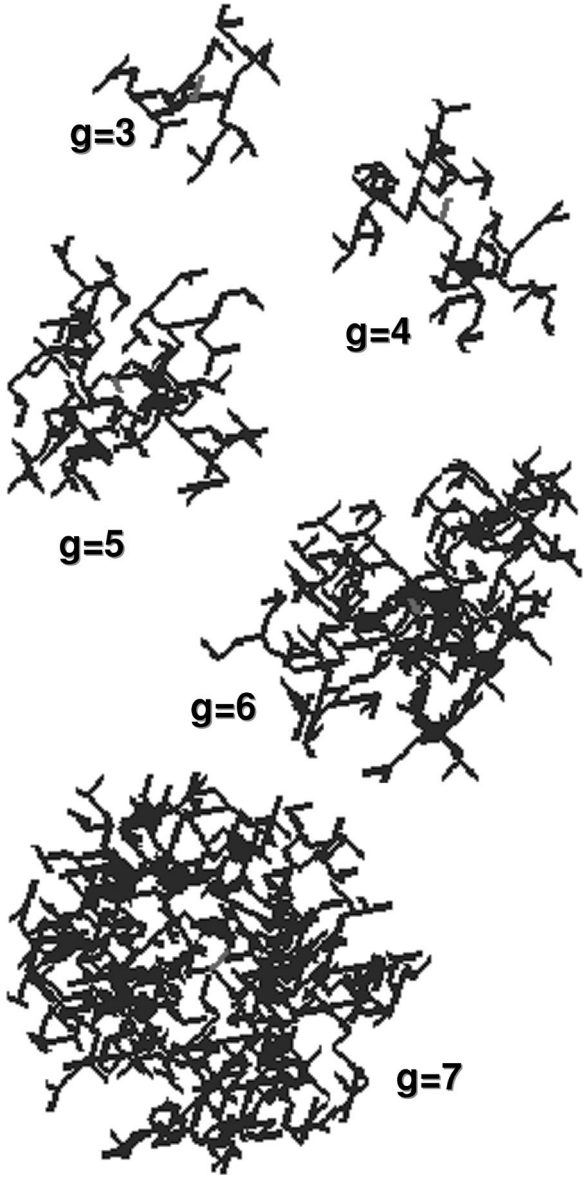

FIG. 2. Snapshots of the equilibrated simulated structures for dendrimers with generations $g = 3-7$.

Moving the systems continuously by means of the cooperative rearrangements characteristics of the CMA, a large number of conformations have been generated for each structure. The following quantities characterizing dimensions and details of the segment distributions in simulated dendrimers were determined as averages over the variety of states considered to be belonging to equilibrium.

(1) Distributions of beads around the center-of-mass $\rho(r)$, as well as the distributions of the free ends $\rho_e(r)$, representing fractions of lattice sites occupied by dendrimer beads within spherical shells of radius r centered at the center-of-mass.

(2) Site-site correlation function of sites separated by $r = r_i - r_j$

$$\gamma(r) = \frac{1}{N}\langle c_k(r_i) \cdot c_l(r_j)\rangle, \tag{9}$$

where N is the total number of beads constituting the dendrimer, c_k and c_l are contrast operators assuming values of 1 for sites occupied by molecular elements (beads) and assume 0 everywhere else.

(3) Mean square radius of gyration

$$\langle R_g^2\rangle = \langle (r_i - r_{\mathrm{cm}})^2\rangle, \tag{10}$$

where r_i and r_{cm} are space coordinates of monomers and the centers of mass, respectively.

(4) Mean square center-to-end-bead distance

$$\langle R_e^2\rangle = \langle (r_{e,i} - r_c)^2\rangle, \tag{11}$$

where $r_{e,i}$ and r_c are the coordinates of the end and center bead(s) which are marked by the empty and striped bead(s) in Fig. 1(b), respectively.

(5) Static form factor

$$P(q) = \sum_{ij} \gamma(r) \frac{\sin(qr)}{qr}, \tag{12}$$

where q is the scattering vector.

The sizes and distances are expressed in units $[a]$ having length of half of the fcc lattice constant; accordingly the bond length is $a\sqrt{2}$.

III. RESULTS AND DISCUSSION

A. Form factor

We would like to start the discussion of our results with the quantity intrinsically measured by a small-angle scattering experiment, the particle form factor $P(q)$.

The generation dependent changes in the form factor have been measured with SAXS on PAMAM dendrimers by Prosa *et al.*[2] ($g=0-10$) and Mallamace *et al.*[3] ($g=1-8$). In addition there are some SANS and SAXS results on low-generation dendrimers of different type, including poly(benzyl ether) (Kleppinger *et al.*,[4] $g=0-2$ and Evemenko *et al.*,[5] $g=1-5$), poly(propyleneimine) (Scherrenberg *et al.*,[6] $g=0-4$), poly(propyleneamine) (Ballauff and co-workers,[7,8] $g=3-4$) and poly(allylcarbosilane) (Kuklin *et al.*,[9] $g=3-5$) dendrimers.

All experimental results, in respect to the appearance of higher order maxima for high-generation ($g \geqslant 5$) dendrimers[13–17] and the scattering contribution of the internal density fluctuations at high scattering vectors[13,14,16–19] are in very good qualitative agreement with results obtained from various computer simulations.

However, theories assuming Gaussian interaction between segments for the calculation of the form factor cannot describe the development of higher order maxima (Wallace *et al.*,[18] Boris and Rubinstein,[47] La Ferla,[48] Hammouda,[49] Burchard[50]). They predict much looser structures in particular for high-generation dendrimers.

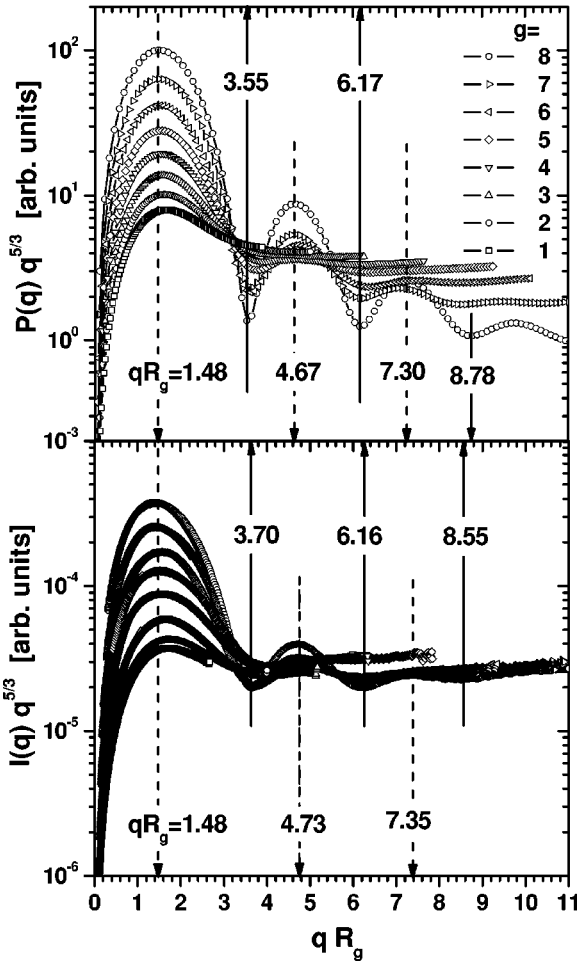

FIG. 3. Bottom: SAXS spectra for dendrimer generation $g=1-8$ in a generalized Kratky presentation (markers). Top: Form factors obtained from computer simulations for the same dendrimer generations in a analogous representation. The solid vertical lines mark the locations of the minima and maxima in the spectra obtained for the $g=8$ dendrimers.

Figure 3 shows a comparison between our SAXS spectra for all dendrimer generations obtained at low polymer concentration ($c=1$ wt %) with the particle form factors determined by CMA for the simulated single dendrimers. The scattering data shown represent the form factors $P(q)$ since further dilution did not result in a change of the spectra. Hence any influence of interparticle interaction can be considered to be negligible at this small but finite concentration. Both, the experimental and simulation results are presented in form of a Kratky plot generalized for good solvent conditions. The logarithmic Kratky presentation ensures a very sensitive visualization over a broad q range and allows a direct comparison between the scattering spectra and the simulated form factors. The variable of the x-axes qR_g is unit-less with R_g determined by IFT from the scattering spectra and by FT from the simulated pair correlation functions. The intensities are plotted in arbitrary units and the y-axes are only adjusted to show equal number of decades. In

this way the comparison between the scattering data and the simulated spectra is made without any adjustable parameters.

It is seen that all features of the measured spectra are very well reflected in the form factors determined for the simulated systems. For a better comparison the maxima and minima are marked for the $g=8$ dendrimer in both, the simulated and the measured data set. For high-generation dendrimers ($g \geqslant 6$) the first maximum appears between $1.48 \leqslant q \leqslant 1.51$ for the real dendrimers and between $1.48 \leqslant q \leqslant 1.52$ for the simulated dendrimers, which is close to the value of 1.49 expected for homogenous spheres. For the lower generations the maxima shift towards higher values up to 1.66 and 1.67 for the real and simulated $g=3$ dendrimers, respectively. In the simulated and measured form factors secondary maxima become visible from the fifth, and ternary maxima appear from the sixth generation on. For homogeneous spheres the minima, $q_{\min}R_g=\sqrt{3/5}(2n+1)\pi/2=3.65$, 6.08, and 8.52 (with n being a positive integer), are a sensitive measure for the size of the spheres. In agreement with the SAXS results of Prosa *et al.*,[2] the minima found for the simulated and real $g=8$ dendrimers are very close to the values expected for homogeneous spheres. All these observations support the picture of high-generation dendrimers ($g \geqslant 5$) being rather compact, globular objects. Very good agreement between experiment and simulation is not only observed in respect to the location of the minima and maxima but also the variation in the intensity with the generation number is very similar for, both, the real and simulated systems.

Scattering originating from density fluctuations on small length scales dominates the form factor obtained from simulation and scattering experiment at high scattering vectors. The scattering intensity follows a $q^{-5/3}$ power-law dependence as expected for linear polymers under good solvent conditions. In the generalized Kratky presentation this leads to a smearing out of the higher order maxima and to a leveling of the form factor to a plateau for $qR_g \geqslant 3.5$, in particular evident for dendrimers with generations smaller than five. Prosa *et al.*[2] and Mallamace *et al.*[3] discuss a transition from a q^{-4} to $q^{-5/3}$ power-law decay with decreasing dendrimer generation for the high-q region which is accompanied by a disappearance of higher order maxima. The authors interpret their results as a transition from a rather compact, spherical shape of high-generation dendrimers to a much, looser starlike shape of low-generation dendrimers. However, in a previous publication[10] we have shown that the high-q scattering is dominated by contributions originating from internal density fluctuations yielding a $q^{-5/3}$ power-law decay (for good solvent conditions). The relative contribution of this power-law scattering to the overall scattering decreases strongly with increasing generation. As a consequence, and due to the appearance of higher order maxima, the power-law decay is less pronounced in the q window of the scattering experiment for high-generation dendrimers and is not (necessarily) a consequence of changes in the overall shape of the dendrimers.

B. Density profile

Applying self-consistent field theory de Gennes and Hervet[51] were the first to perform a theoretical study on the structural properties of dendrimers. They predicted a monomer density profile with a minimum in the center and monotonically, increasing density towards the dendrimer periphery. Congestion in the outer shell with increasing generation yields a critical generation above which perfect growth of the dendrimer is impossible. However, Boris and Rubinstein[47] later on showed that this result is not a consequence of the self-consistent field approach but rather is a consequence of the assumption that the monomers of each generation are constricted to concentric shells. Relaxing this constriction, the numerical self-consistent field approach of Boris and Rubinstein[47] yields a Gaussian-like density profile having the maximal density at the center of the molecule, but no plateau, with a monotonic decrease of the density towards the edges. In a recent publication Zook and Pickett[52] generalized the approach of de Gennes and Hervet[51] by overcoming their *a priori* assumption that a single dendrimer conformation where the monomers of each generation are constricted to concentric shells dominates the thermodynamic limit. In the limit of long, flexible spacers between branching points they obtain parabolic density profiles with a dense core for high generation ($g \geqslant 5$) dendrimers. However, for short spacers the authors found numerically a small dip in the density profile at the core of the molecule.

On the basis of the observations outlined in Sec. III A, experimental findings seem to support the picture of dendrimers being rather compact, globular objects.

In order to obtain further details from our scattering experiments, the measured scattering spectra are described by a model which takes into account the scattering stemming from the internal density fluctuations as well as from the overall globular shape of the dendrimers. As described in Sec. II B we used a combination of two terms [see Eq. (6)]: (1) a shape contribution to the scattering obtained from the density profile of a homogeneous sphere of radius R_s with a smeared surface region of width $2\sigma_s$ given by Eq. (7) (see also insert of Fig. 5 in Ref. 10) and (2) a term taking into account the scattering from the internal density fluctuations as given by Eq. (8) with the range of the internal density fluctuations ξ as adjustable parameter. ξ does not vary significantly or systematically with generation and has been determined to be about 1.5 ± 0.1 nm. The segment density profile $\rho(r)$ can be derived from the static form factor $P(q)$ using this model and by a model independent approach using an IFT and a SQDEC algorithm described in more detail in Sec. II B. For dendrimers with generation $g=3-8$, $\rho(r)$ is plotted in the bottom part of Fig. 4 versus the radial distance from the dendrimer center-of-mass normalized to the radius of gyration of the $g=8$ dendrimer. The stepped lines denote the numerical results obtained by the IFT and SQDEC procedures whereas the continuous lines show the results from the model fit. The widths of the steps in the density profiles obtained numerically are a measure for the resolution of the scattering experiment in real space [see Eq. (5)]. Within the error bars of the method the segment density is homogeneous in the center region, exhibits a pronounced plateau, and de-

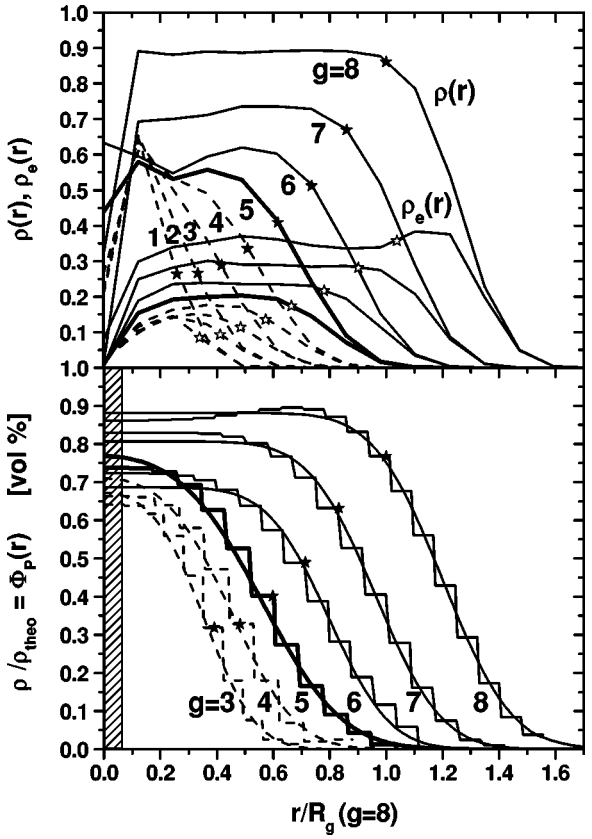

FIG. 4. Segment- $\rho(r)$ and end-group density profiles $\rho_e(r)$ as a function of the radial distance from the center-of-mass normalized to the radius of gyration of the simulated and real $g=8$ dendrimer, respectively. The top part shows the simulation results for dendrimers of generation $g=1-8$. The bottom part presents the results for $g=3-8$ obtained from the SAXS spectra by IFT and SQDEC by stepped lines. The continuous lines mark the results obtained by the model fit described in the text. The hatched area marks the resolution limit of the IFT and SQDEC method. The full and open stars mark for each generation the condition $r=R_g$ and $r=R_e$, respectively.

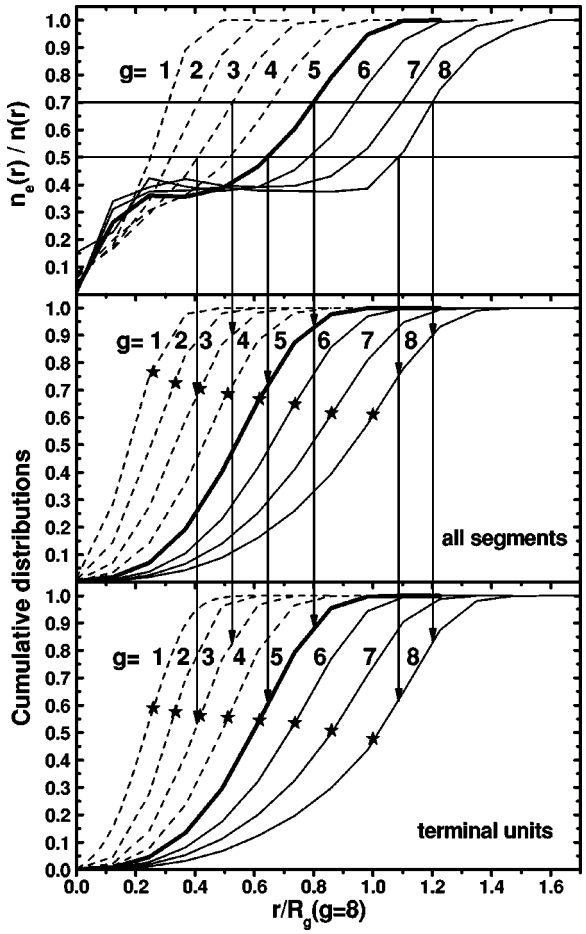

FIG. 5. Number of end groups n_e normalized to the overall segment number n at a certain radial distance r from the center-of-mass vs r normalized to the radius of gyration of the $g=8$ dendrimer (top). Cumulative distributions of all segments $\Sigma_{r_i \leqslant r} N_i(r_i)/N$ and the terminal units only, $\Sigma_{r_i \leqslant r} N_{e_i}(r_i)/N_e$, are shown in the middle and bottom part, respectively. The full stars mark the conditions $r=R_g$ for each generation. The solid lines in the top part mark the condition $n_e(r)/n(r)=0.5$ and 0.7. The arrows assign these conditions to the corresponding locations on the cumulative distributions.

creases monotonically to zero in a smeared outer surface region. The absolute values of the segment densities in the dendrimer center are rather high. Polymer concentrations of about 0.9 vol % are found for the $g=8$ dendrimer which decreases slightly from 0.8 vol % for the $g=7$ dendrimer to about 0.7 vol % for the dendrimers with generations $g=3-6$. A significant change in the density profiles occurs between the fifth and sixth generation. This change is best indicated by plotting the relative width $2\sigma_s/R_s$ of the surface region, shown in Fig. 5 of Ref. 10, as a function of the generation. The relative width of the surface region increases drastically, stepwise from 28% to 48%, when the generation is decreased from $g \geqslant 6$ to $g \leqslant 5$.

The Gaussian density profile obtained for $g=3$ and 4 dendrimers by Ballauff and co-workers[7,8] from small-angle neutron scattering experiments (SANS) are in good qualitative agreement to the much more extended decay of the density profiles found by us for the low-generation dendrimers $g \leqslant 5$. The rather extended, very dense plateaus and monotonic, rapid decrease of the segment density in the smeared surface region with increasing generation as obtained from our experiment are similar to the SAXS results reported by Prosa *et al.*[2] ($g=3-9$) but differ for lower generations $g \leqslant 5$ in respect to a local density minimum in the dendrimer periphery observed by Prosa *et al.*

For a comparison between simulation and experimental results the density profiles obtained from the simulation are plotted in the top part of Fig. 4 in the same manner. In Figs. 4 (and 5), the bold solid line marks the results obtained for the fifth generation, thin dashed lines and thin solid lines mark the results obtained for generation $g \leqslant 4$ and $g \geqslant 6$, respectively. The simulation reproduces the generation dependent development of the profiles, derived from the experimental results, very well. The simulated profiles exhibit a pronounced plateau for high-generation dendrimers. The plateau densities are rather high and show the same trend as the results based on the experiment. The plateau values decrease from about 0.9 vol % for $g=8$, over 0.7 vol % for $g=7$ to about 0.6 vol % for the $g=5$ and $g=6$ dendrimers. Compared to the experimental results, the final decay towards the outer edges is somewhat steeper in the profiles of the simulated dendrimers. Plateaus extend to radial distances of about $r \approx R_g$ in the simulated profiles but only to about $r \approx 0.8 \times R_g$ for the real system. For $g \leqslant 4$ the plateaus disappear

and a more gradual decay to the outer edges is observed. The major difference between profiles obtained from the scattering spectra and from simulation is the small density hole at the dendrimer center observed in the simulated profiles. However, the dimension of this density hole is certainly at the resolution limit $\Delta r \approx 0.3$ nm of the scattering experiment, marked by the hatched area in Fig. 4 (bottom). A significant change in the density profiles is observed between the fifth and sixth generation for the real system and for the simulated dendrimers between the fourth and fifth generation. This shift in generation might be attributed to the slightly different core structures (see Fig. 1).

Computer simulations of Lescanec and Muthukumar[20] ($g=0-6$) using a kinetic growth algorithm which might not reflect the equilibrium structure of dendrimers yield similar density profiles as predicted by the theory of Boris and Rubinstein[47] ($g=1-6$). Density profiles exhibiting a dense core but no plateau region are observed even for high-generation dendrimers. Several simulations performed by Scherrenberg *et al.*[6] [molecular dynamics simulation (MD), $g=0-4$], Mansfield and co-workers[13,14] [Monte Carlo simulation (MC), $g=1-11$], Karatasos *et al.*[15] (MD, $g=3-6$), Giupponi and Buzza[16] (MC, $g=3-8$), Timoshenko *et al.*[17] (MC, $g=1-7$, shown $g=4$, 6), Murat and Grest[21] (MD, $g=1-8$, shown $g=5-8$), Lyulin *et al.*[22,23] [Brownian dynamics simulation (BD), $g=0-6$], Lue[24] (MC) ($g=2,4$), Chen and Cui[25] (MC, $g=0-8$) and Cavallo and Fraternali[26] (MD, $g=0-4$) come to a different conclusion. The density, which is always highest at the center (except in Ref. 15), decreases monotonically towards the edges for low-generation dendrimers but for high-generation dendrimers the density profiles exhibit a broad plateau/shoulder before decaying smoothly to zero towards the outer edges. The width of the plateau increases with increasing generation. The formation of a plateau region with constant density is accompanied by the development of a local minimum close to the center.[6,13–17,21–24,26] These simulation results are principally reflected by experimental findings with the exception of two features. The development of a local minimum close to the center seen in computer simulations for high-generation dendrimers has not been observed in the experiments, neither could the local minima in the dendrimer periphery, as experimentally found by Prosa *et al.*[2] for low-generation dendrimers, be affirmed by computer simulations.

Hence, we can conclude that the increasing width of the plateau with increasing generation and the more gradual decay for low-generation dendrimers obtained from our experiment and simulation are in good qualitative agreement with the results found by other authors by computer simulation[6,13,15–17,21–26] and scattering experiments.[2,7,8]

Some detailed differences between results of different simulations are probably dependent on details of core architecture and on other parameters such as spacer length and coordination at branching points. This can influence to some extent the appearance (location) of the density hole in the center region as seen in our and in other computer simulation results.[6,13,15–17,21–24,26]

The small density drop observed in the center of the simulated dendrimers might be caused by the stretching of the center but is according to our simulations small because of the back-folding of the outer generations. Zook and Pickett[52] proposed for dendrimers with short spacers a small density drop in the close vicinity of the zero generation as observed in the majority of computer simulations. However, it was always found that the density is highest directly in the center. We also performed simulations on dendrimers with longer spacer $P \geqslant 2$ which seem to support the picture that maximal density at the center followed by a local minimum is characteristic for longer, more flexible spacers.[53] Indeed, most of the computer simulations on dendrimers have been performed on dendrimers with spacer length larger than $P=1$ (Refs. 13, 14, 16, 17, 21) or resolving the spacer on an atomistic (corse-grained) level.[6,26,27] We found that the simulation data for $P=1$ yield best agreement with the results from the scattering experiment despite the density hole at the center which is certainly beyond the resolution limit of the scattering experiment.

The dendrimers probably can anyway be used as a box/cage because back-folding peripheral elements might be pressed out by an foreign molecular object in the center and, hence, will increase the outer density which can constitute enough high barrier for the object to escape from the so formed cage.

Stretching of the first generations can also be considered as responsible for correlations between the first generations resulting in density peaks as seen by some authors.[13–15,19,25] The absence of density peaks in our results is caused by different normalization methods used and to some extent also by differences in stiffness or intramolecular flexibility of the model systems. The densities determined here represent fractions of lattice sites within spherical shells of radius r centered at the center-of-mass and having thickness Δr comparable with the bond length. Such normalization in the case of a lattice model takes already into account that the systems locally are not continuous and the normalized density just reflects which fraction of available sites is occupied (as seen on length scales addressed by a small-angle scattering experiment). If, however, in such systems the normalization would be made with respect to available continuous space the distribution should reflect the discrete character of the lattice and a nonuniform distribution of elements at short correlation distances would follow. This can nicely be seen by comparing the results of Mansfield[13] to an earlier publication of the same author.[14] Density distributions determined here for dendrimers can also be compared to distributions determined for other macromolecules simulated by this method.[45,46]

Furthermore, the discrete nature of the local arrangement of elements should be considerably smeared out when the flexibility of the dendrimer is large and consequently the center-of-mass strongly fluctuates with respect to positions of the elements near the topological center of the dendrimer. As a consequence coordination peaks should be significantly smeared out when the density is plotted relative to the center-of-mass rather than relative to the core bead.[13–15,25] The dendrimers considered in this publication are extremely flexible. They consist of elements which in the linear configuration have a persistence length smaller than two bonds.[44] Unfortu-

nately, in the simulation of Harreis *et al.*[19] in which the density distributions show a strong discrete character of local correlations the persistence length is not known but can be supposed to be much larger considering the observed effects which may result from the structure stiffness. The large flexibility of the dendrimers in the here presented systems is achieved due to the cooperative mobility of the dendrimer elements even under conditions of high local density and high branching degree. Certainly, this example contradicts opinions that simulations on lattices represent more stiff systems.

C. Location of the end groups

Concerning the location of the end groups, Ballauff and co-workers[7] derived the end-group distribution from small-angle neutron scattering experiments on a deuterium end-labeled $g=4$ dendrimer using contrast variation. Their findings led to the conclusion that the outer generation can be found all over the dendrimer interior since the end-group distribution could be described by a Gaussian. Topp *et al.*[11] measured the radius of gyration of the outer generation on a contrast matched end-labeled $g=7$ dendrimer. From the fact that the radius of gyration of the end groups $R_{g,e}$ is larger than R_g of the corresponding unlabeled dendrimer, the authors concluded that most of the terminal units are located near the dendrimer periphery. Lyulin *et al.*[22] later questioned the validity of this conclusion since segment distributions can be constructed yielding $R_{g,e}>R_g$, with most of the terminal units located in the interior of the dendrimer. All computer simulations cited so far including the simulation of Harreis *et al.*[19] (MC, $g=3$) and Lee *et al.*[28] (MD, $g=2-6$) as well as the theoretical work of Boris and Rubinstein[47] and Zook and Pickett[52] come to the conclusion that there is significant back-folding of the end groups and that the terminal units can be found all over the interior of the dendrimers except for a small depletion zone close to the center. The simulations of Karatasos *et al.*[15] and Timoshenko *et al.*[17] yield end-group distributions showing that the terminal units even can approach the center of the dendrimer. The end-group distributions derived by Boris and Rubinstein[47] exhibit off-centered peaks and have a rather Gaussian-like shape. Computer simulations of Mansfield[13] and Giupponi and Buzza[16] obtain end-group density profiles with a peaklike shape for low dendrimer generations. However, for high generations they observe a plateau at intermediate radial distances. In accordance to the overall segment distribution the extension of the plateau increases as the dendrimer generation is increased. The simulations of Murat and Grest[21] as well as the results of Lyulin *et al.*[22] confirm the plateaulike shape of the end-group density profiles for high-generation dendrimers. End-group distributions obtained by Scherrenberg *et al.*[6] and Karatasos *et al.*[15] exhibit peaks at larger radial distances with a rather extended shoulder towards the dendrimer center. The molecular dynamics experiments of Cavallo and Fraternali[26] and Mazo *et al.*[27] ($g=4$) on dendrimers with, however, rather bulky end groups come to somewhat different conclusions. Mazo *et al.*[27] found the terminal units to be localized at the periphery and only about 20% of the end groups are situated in the internal region of the dendrimer. Increasing bulkiness of the terminal units shifts the peak of the end-group distribution closer to the outer edge. Cavallo and Fraternali[26] found the end groups to be rather localized at the surface for $g\leqslant 2$ but in accordance with other authors[6,15] for $g\geqslant 3$ end-group distributions develop a shoulder towards the dendrimer center but the terminal units are still expelled from the core region.

Mansfield,[13] Karatasos *et al.*,[15] and Murat and Grest[21] resolved the distributions for individual subgenerations $g'\leqslant g$ in dendrimers of various generations g relative to the center bead. The subgenerations close to the core are found to be rather localized (relative to the center bead) whereas the outer subgenerations are delocalized and can be found all over the dendrimer interior (except the core region). For high-generation dendrimers the peaks for the inner subgenerations $g'<5$ shift to larger radial distances and become sharper with increasing generation indicating enhanced stretching of the inner subgenerations. Subgenerations $g'\geqslant 5$ remain delocalized with distributions showing a broad shoulder/plateau towards the dendrimer center. Driven by excluded volume interaction the inner generations stretch out to gain volume to enable the outer generations to fold back. Since only a small fraction of the mass is located in the center, the entropic penalty paid is only small and it is entropically more favorable to enable the outer parts of the dendrons, where most of the mass is located, to adopt a more coiled conformation. This mechanism is also confirmed by Timoshenko *et al.*[17] for dendrimers with $g\geqslant 4$ by looking at the mean-square distance between radial neighbors.

The local minimum found by the majority of the simulations[6,13–15,17,21–24,26] in the overall monomer density distribution close to the core has been explained by an incomplete refill of the vacancies created by stretching the inner generation through the back-folding of the outer generations.

The distributions of the terminal units obtained from our simulation are included in the top part of Fig. 4. We consent with the majority of authors that for all generations the end groups can be found all over the dendrimer except in a small depletion zone at the dendrimer centers. End-group distributions for high generations exhibit broad plateaus[13,15,16,21,22] which are, compared to the distributions obtained for all segments, somewhat more extended towards larger radial distances from the center. End-group distributions obtained for dendrimer generations lower than $g=5$ do not show plateaus but exhibit a rather peaklike shape.[7,13,16,19]

In accordance to the overall segment distributions, for the end-group distributions a general change in shape is found to take place between the fourth and fifth generation.

For a more quantified discussion of the generation dependent changes in the distribution of the terminal units, the number of end groups relative to the overall segment number $n_e(r)/n(r)$ and the cumulative distributions of terminal units and all segments are plotted in Fig. 5 as a function of the radial distance from the center of mass normalized to the radius of gyration of the $g=8$ dendrimer. For $g\geqslant 5$, $n_e(r)/n(r)$ develops a distinct shoulder towards smaller radial distances. Evidently, for generations $g\geqslant 5$ enhanced back-folding of the end groups towards the dendrimer center

TABLE II. Percentage of all segments and terminal units located in the ''interior'' of the dendrimers if the interior is defined by $n_e(r)/n(r) \leqslant 0.5$, 0.6, 0.7, and 0.8, respectively.

	$n_e(r)/n(r) \geqslant 0.5$			$n_e(r)/n(r) \geqslant 0.6$			$n_e(r)/n(r) \geqslant 0.7$			$n_e(r)/n(r) \geqslant 0.8$		
g	r/R_g	N (%)	N_e (%)	r/R_g	N (%)	N_e (%)	r/R_g	N (%)	N_e (%)	r/R_g	N (%)	N_e (%)
1	0.97	71	56	1.08	81	66	1.20	87	77	1.31	91	86
2	0.96	69	53	1.10	83	69	1.24	89	79	1.37	94	89
3	0.98	69	54	1.13	82	72	1.27	91	83	1.40	96	92
4	1.01	70	56	1.16	84	75	1.29	92	87	1.41	97	96
5	1.05	72	60	1.19	87	79	1.30	93	88	1.40	98	96
6	1.07	74	63	1.19	87	79	1.28	93	88	1.36	98	95
7	1.10	75	65	1.20	86	78	1.28	95	90	1.35	97	94
8	1.09	75	62	1.15	83	72	1.20	90	83	1.27	95	91

takes place. The enhanced back-folding of the terminal units is accompanied with the appearance of a pronounced plateau in the (end-group) density profiles and is in accordance with the observations of Mansfield,[13] Timoshenko *et al.*,[17] and Murat and Grest[21] that the inner part of the dendrimer stretches out for high-generation dendrimers to allow outer generations to adopt an entropically more favorable conformation through folding back into the vacancies.

Following the evaluation of Luylin *et al.*[22] we now would like to address the question which fraction of the end groups is located at the dendrimer surface or interior, respectively, in a more quantitative manner as a function of the dendrimer generation. The cumulative distributions $\Sigma_{r_i \leqslant r} N_i(r_i)/N$, shown in the middle part of Fig. 5, give the number of all units located at distances r_i smaller or equal r relative to the overall number of units in the dendrimer. In the bottom part of Fig. 5, the analogous cumulative distribution $\Sigma_{r_i \leqslant r} N_{e_i}(r_i)/N_e$ for the terminal units is presented. If we now define the interior of a dendrimer by the condition $r \leqslant R_g$, corresponding to the extension of the plateaus of the density profiles of high-generation dendrimers, about 60% ($g=8$) to 70% ($g=3$) of all segments but also 47% ($g=8$) to 56% ($g=3$) of all end groups are located in the interior of the dendrimer. Another approach might define the dendrimer periphery by the condition that the end groups should be the dominating species, thus $n_e(r)/n(r)$ should exceed 50%. In the top part of Fig. 5, the condition $n_e(r)/n(r)=0.5$ and 0.7 are marked by the solid lines. The arrows mark the corresponding points on the cumulative distributions for the $g=3$, 5, and 8 dendrimers. From the rather relaxed condition $n_e(r)/n(r) \geqslant 0.5$, we obtain that about 46% ($g=3$) to 35% ($g=7$) of the terminal units are located in the periphery of the dendrimer. However, getting somewhat more restrictive with $n_e(r)/n(r) \geqslant 0.7$, we obtain that only 10% ($g=7$) to 17% ($g=3, 8$) of the end groups are located at the dendrimer surface. We, therefore, would like to conclude that at least for these rather flexible dendrimers a significant fraction of the terminal units is not located at the dendrimer surface. Table II summarizes the results for all generations for the conditions $n_e(r)/n(r) \geqslant 0.8$, 0.7, 0.6, and 0.5.

D. Radius of gyration and fractal growth of dendrimers

Another question tried to be answered by computer simulations as well as by scattering experiments has been whether dendrimers grow in a fractal manner or not. Dendrimers can be considered as fractal, growing objects if the addition of a new generation to a dendrimer (i.e., increasing its molecular mass M_w) leads to self-similar structures for which the radius of gyration scales with $R_g \propto M_w^{1/D} = M_w^{\nu}$, where ν denotes the Flory exponent and D is the fractal dimension. Hence, from the molecular weight dependence of the dendrimer dimensions conclusions can be drawn whether or whether not dendrimers grow in a self-similar manner when a new generation is added.

Some computer simulations (Scherrenberg *et al.*,[6] Karatasos *et al.*,[15] Giupponi and Buzza,[16] Murat and Grest,[21] Lyulin *et al.*,[23] Cavallo and Fraternali[26]) as well as scattering experiments [Evmenenko *et al.*[5] ($g=1-5$), Scherrenberg *et al.*,[6] Prosa *et al.*[12] ($g=2-9$)] obtain a fractal dimension of $D \approx 3$ indicating that dendrimers are compact, space filling (homogeneous) structures. The Monte Carlo simulations of Lue[24] on dendrimers under good solvent conditions yield values between $\nu \approx 0.67$ ($D \approx 1.49$) and 0.60 ($D \approx 1.67$) depending on the size of the beads from which the dendrimers are build. A fractality $D > 3$ would indicate that the mass added by a new generation is predominately located in the periphery as assumed by the theory of de Gennes and Hervet.[51] Below a critical generation de Gennes and Hervet[51] obtain $R_g \propto M_w^{0.20}$ ($D=5$), which is close to the exponent of $\nu = 0.25$ ($D=4$) as expected for a perfect Cayley tree derived by Zimm and Stockmeyer.[54] Above the critical generation, the radius of gyration scales with the molecular weight with $D=3$ as expected for compact, homogeneous objects. Computer simulations of Wallace *et al.*[18] (MC, $g=1-5$) as well as of Lescanec and Muthukumar[20] yield $R_g \propto P^{0.5} M_w^{0.22}$ ($D=4.54$). Surprisingly, density profiles obtained by Lescanec and Muthukumar[20] are clearly monotonically decreasing towards the periphery. Unfortunately, Wallace *et al.*[18] do not show any results on the density profiles. Monte Carlo simulations of Mansfield[13] show a variation of the fractality from $D=1.64$ to 2.79 as the dendrimer genera-

tion is increased from $g=1$ to 8. The dendrimers become more compact with increasing generation but the result $D<3$ suggests somewhat looser structures than solid spheres ($D=3$). Mallamace *et al.*[3] ($g=1-8$) report results from scattering experiment on PAMAM dendrimers and molecular dynamics simulations. For low-generation dendrimers they observe a fractal dimension of about $D\approx 2.4\pm 0.4$, which is in the same range as the values obtained by Mansfield.[13] However, for high-generation dendrimers they obtain $D\approx 4.8\pm 0.4$, which would be in accordance with the scaling behavior found by Wallace *et al.*[18] and Lescanec and Muthukumar.[20] Hydrodynamic radii obtained for PAMAM dendrimers from dynamic light scattering experiments by Stechemesser and Eimer[55] ($g=2-10$) do not show a clear scaling behavior of the dendrimer dimension with the overall molecular weight. This finding is in (qualitative) agreement with the results of Mansfield,[13] Chen and Cui,[25] Sheng *et al.*[29] ($g=1-7$) and Carl[56] ($g=2-8$) obtained from Monte Carlo simulations.

From a generalized Flory approach (using self-consistent free energy minimization) Sheng *et al.*[29] obtain for the radius of gyration

$$R_g \propto \begin{cases} N^{1/5}(g+1)^{2/5}P^{2/5} & \text{for good solvent} \\ (g+1)^{1/2}P^{1/2} & \text{for } \theta \text{ solvent} \\ N^{1/3} & \text{for bad solvent} \end{cases}, \qquad (13)$$

where N and P are the total number of segments in the dendrimer and P the number of segments between the branching points (here starburst dendrimer $P=1$), respectively. The authors confirm their theory using results from Monte Carlo simulations. Only for collapsed structures in bad solvent scaling with N as expected for a homogeneous, compact object is found. The Gaussian size of a dendrimer is of the order of the size of a linear strand of $(g+1)\times P$ monomers.[29,47] The scaling relation found for good solvent describes very well the theoretical results obtained by Ganazzoli *et al.*[57] ($g=0-6$) for high generations and is identical to the results of Boris and Rubinstein[47] derived from their Flory approach. The analytical formulas derived by Boris and Rubinstein,[47] La Ferla[48] (special case $m=2$, $f=3$, $P=1$), and Carl[56] (special case $m=f-1$) for the radius of gyration of a Gaussian dendrimer reduce to Eq. (13) for θ conditions in the limit $m^{g+1}\gg 1$ and $P\gg 1$. Zook and Pickett[52] obtain in the framework of their self-consistent field approach $R_g \propto N^{1/5}P^{2/5}$ under excluded volume conditions.

On the basis of their Monte Carlo simulation results Chen and Cui[25] suggested for large g a generalized relation for the radius of gyration in terms of the Flory exponent ν

$$R_g \propto N^{(2\nu-1)}[(g+1)P]^{(1-\nu)}. \qquad (14)$$

Equation (14) reduces to Eq. (13) with $\nu=3/5$ and 1/2 for good and θ solvent, respectively. On the basis of Monte Carlo simulations and simulations using the Gaussian self-consistent method, Timoshenko *et al.*[17] propose for the dendrimer radius of gyration a relation involving two exponents: $R_g \propto P^{(\nu-\nu')}N^{\nu'}$, where $\nu'\approx\nu\approx 1/3$ for bad solvent conditions and $\nu'\approx\nu-1/4\approx 0.338$ calculated with $\nu=0.588$, the Flory exponent for good solvent conditions obtained from perturbation calculations.[58]

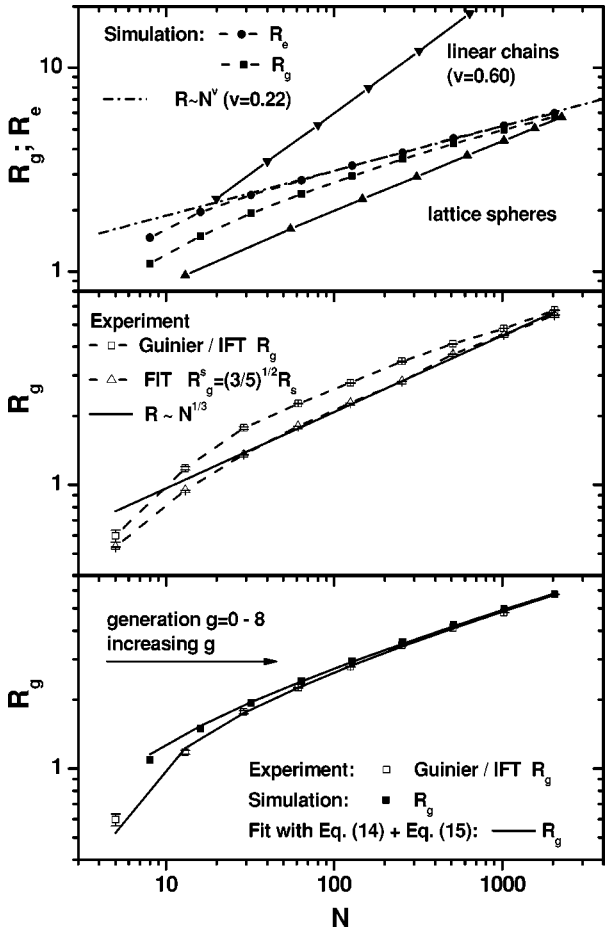

FIG. 6. Dendrimer dimensions as a function of the overall segment number for dendrimers of generation $g=0-8$ in double-logarithmic presentation. Top: Radii of gyration (full squares) and center-to-end-bead distance (full circles) are presented. For comparison the dependency for simulated linear chains (full triangles down) and lattice spheres (full triangle up) are also shown. The dash-dotted line marks the power-law dependence $R\propto N^{0.22}$. Middle: Comparison of the radii of gyration obtained from the SAXS data by IFT and Guinier analysis (open squares) and calculated from the sphere radii obtained from the model fit (open triangles). The solid line marks the dependence $R\propto N^{1/3}$ expected for solid, three-dimensional objects with generation independent density. Bottom: Comparison of the radii of gyration obtained from simulation (solid squares) and from the SAXS data by IFT and Guinier analysis (open squares). Solid lines show results of a fit using Eqs. (14) and (15).

First we would like to discuss the results obtained for the simulated dendrimers. In the simulated system the mass is given by the total number of beads in the given structure and the size can be characterized by the radius of gyration or by the mean distance of free ends from the dendrimer center. Figure 6 shows dependencies of the radii of gyration and the center-to-end-bead distances versus the total number of beads for dendrimers with generations $g=0-8$; data are summarized in Table I. For comparison the dependencies of the radii of gyration for flexible linear chains and for lattice spheres (dense packed beads on the lattice) are presented in the top part of Fig. 6. The simulated systems were modeled to represent good solvent conditions. The characteristic scal-

ing of the linear chain dimensions, $R_g \propto N^{\nu}$ with $\nu=0.6$, is well reproduced. The corresponding scaling for compact lattice spheres is well described by the exponent $\nu=1/3$. The comparison between results obtained for dendrimers, linear chains, and lattice spheres show that the dimensions of dendrimers are always between the extremes described by the loosely packed linear chains and compact spheres. Dendrimers of small generations have dimensions closer to those of linear chains. Increasing the generation makes them much more compact with dimensions closer to those of compact spheres. It can be noticed from the top part of Fig. 6 that the $g=8$ dendrimer has almost the size of a compact lattice sphere. This is in agreement with the experimental and simulated results for the density profiles where densities close to one were obtained in the center of the dendrimer (see Sec. III B).

Let us now turn to the experimental results. In the middle part of Fig. 6, the radii of gyration determined from the scattering data via IFT ($g \geqslant 3$) or Guinier analysis ($g<3$) are plotted as a function of the total number of monomers; values are summarized in Table I. The radii of gyration $R_g^s=\sqrt{3/5}R_s$ of the analogous, homogeneous spheres with the same mass and the same density in the center region as the real dendrimers where calculated from the R_s determined from the model fit of the scattering spectra [see Eq. (7) and in Ref. 10 the insert of Fig. 5] and are also included in the middle part of Fig. 6. Despite (small) deviations due to changes in the dendrimer core densities, R_g^s follows very well the expected 1/3-power-law behavior for generations $g \geqslant 3$. The density changes of about 30% are suppressed compared to the exponential growth of the mass with generation. As for the simulated system the dendrimer radius of gyration is always larger than the radii of the analogous, homogeneous spheres, but the values nearly approach each other for the $g=8$ dendrimer.

Finally, the bottom part of Fig. 6 shows a comparison between the radii of gyration obtained for the simulated dendrimers and for the real system. The simulated data are shifted in such a way that the radius of gyration of the simulated $g=8$ dendrimer equals the corresponding experimental value. For $g=8$ deviation due to the different core structures should be minor. Except for deviations for the lowest generations which can be attributed to the different core structures very good agreement between simulation and experiment is obtained. Obviously, no scaling of R_g with the total number of segments N is found.

These findings are in (qualitative) agreements with the computer simulations of Mansfield,[13] Chen and Cui,[25] Sheng *et al.*,[29] and Carl[56] and the experimental results of Stechemeier and Eimer[55] but not in accordance with the conclusion drawn by the majority of authors[5,6,12,15–18,20,21,23,24,26] who discussed their results in terms of simple power-law dependence on N. However, various theoretical approaches (except Zook and Pickett[52]) have shown that the radius of gyration should not follow a simple power-law dependence on N, neither for a Gaussian dendrimer[29,47,48,56] nor under good solvent conditions.[29,57]

The solid lines in the bottom part of Fig. 6 show results of a fit with Eq. (14) suggested by Chen and Cui[25] in terms of the Flory exponent ν. The generation g can be expressed by the total number of segments N

$$N=Pf\frac{m^g-1}{m-1}+N_c \Leftrightarrow g=\frac{1}{\ln[m]}\ln\left[\frac{(N-N_c)(m-1)}{Pf}+1\right], \tag{15}$$

where $P=1$ is the number of spacer units, $m=2$ and $f=4$ are the functionalities of the branching units and the core, respectively. N_c denotes the number of segments in the core which is equal to 4 for the simulated or equal to 1 for the real system. For the Flory exponent, we obtain within the error bars identical values $\nu=0.585\pm0.002$ for the simulated and the real dendrimers. The value is very close to the Flory exponent $\nu=0.588$ for good solvent conditions obtained from perturbation calculations for the excluded volume effect.[58] However, the fact that the radius of gyration does not scale with the molecular weight indicates that dendrimers do not grow by adding a new generation in a self-similar manner. Interestingly, for generations $g \geqslant 3$ the center-to-end-bead distance included in the top part of Fig. 6 can be well described by a power law: $R_e \propto N^{0.22}$. The center-to-end-bead distance should be considered as being very similar to the radius of gyration of the end groups. It is surprising that the exponent of 0.22 found in the simulations of Lescanec and Muthukumar[20] for the power-law dependency of the radii of gyration of the overall dendrimers describes the dependency of R_e very well.

E. Pair-correlation function and internal fractal structure of dendrimers

Now we would like to turn to the question whether or whether not the internal structure of dendrimers is fractal, as implied by their architecture. Power-law behavior of the pair correlation function $\gamma(r)$ can be taken as an indication for a fractal substructure. In Fig. 7 the pair correlation functions $\gamma(r)$ obtained by IFT from the scattering data (bottom) and directly determined [see Eq. (9)] for the simulated systems (top) are shown as a function of the intersegment distance normalized to the radii of gyration of the $g=8$ dendrimers in a double-logarithmic presentation. The solid lines represent fits of the initial decay to $\gamma(r) \propto r^{-(3-D)}$, where D is attributed to the fractal dimensions. For a comparison to previous results obtained by Mansfield[13] from Monte Carlo simulations, the generation dependent values are summarized in Table III. D increases monotonically with generation from a value close to $D=5/3 \approx 1.67$ as expected for a linear chain under good solvent conditions up to a value $D \approx 2.78$ close but lower than 3 as expected for compact, space filling objects. The agreement between Mansfield's results and our simulation results is very good. The experimental findings show a weaker generation dependence with systematically lower values for D for $g>3$. Even though the general trend of the results fits very well into the picture of dendrimers changing from a looser, polymericlike conformation to a more globular, compact shape with increasing generation, the results of this analysis should not be overstressed. Since the size of dendrimers is fairly small, the range where the $\gamma(r)$ can be described by power laws is rather limited.

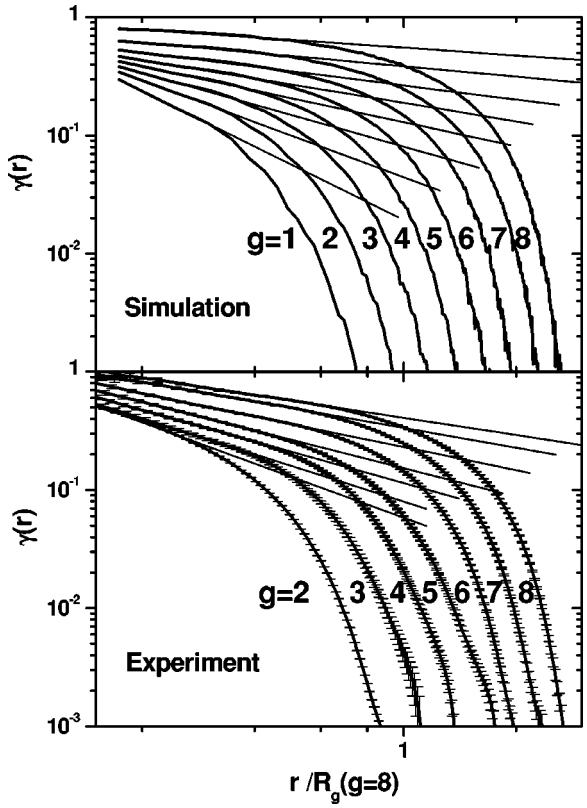

FIG. 7. Double-logarithmic presentation of the pair correlation function $\gamma(r)=p(r)/r^2$ as a function of the segment distance normalized to the radius of gyration of the simulated and real $g=8$ dendrimer, respectively. The top part shows the simulation result for dendrimers of generation $g=1-8$ and in the bottom part the results obtained by IFT from the SAXS spectra are shown for $g=2-8$. Solid lines show results of a fit of the initial decay using $\gamma(r)\propto r^{-(3-D)}$.

IV. CONCLUSIONS

We investigated the shape and the internal structure of starburst dendrimers in dilute solution using SAXS and computer simulation experiments. We compared various quantities characterizing the structure, such as the form factor (intrinsically measured by SAXS), the pair correlation functions, the radial density profiles (intrinsically determined by the simulation), and the dendrimer dimensions. Very good agreement between the simulated and real dendrimers has been observed. The good agreement can be regarded as an indication that the simulation considers properly the strongest interactions controlling the structure, i.e., the excluded volume interaction and the intramolecular (covalent) bonding leading to the specific architecture.

For the interpretation of the scattering data, a model has been formulated which describes the form factor for all dendrimer generations consistently by taking into account the scattering due to internal concentration fluctuations and from the overall shape of the dendrimers. We have shown that the IFT and SQDEC methods are powerful tools to obtain detailed information about the structure of dendrimers in real space from the scattering spectra and provide a valuable crosscheck for data modeling. All characteristic features, such as the development of higher order maxima with increasing generation as well as the power-law scattering stemming from the internal density fluctuations are represented in the spectra of the simulated dendrimers.

The segment density profiles obtained from the scattering data and from the computer simulation clearly show a homogeneous segment density in the center region. For high-generation dendrimers, the profiles show rather pronounced plateaus in the center and decay monotonically to zero in a rather narrow surface region. For low-generation dendrimers the plateaus become more narrow (experiment) or disappear (simulation) and the final decay towards the dendrimer periphery becomes more gradual. The simulation shows a very narrow density hole at the dendrimer center of mass, which is at the resolution limit $\Delta r\approx 0.3$ nm of the scattering experiment.

The computer simulation provides additional information about the location of the terminal units. Despite a small depletion zone at the dendrimer center, terminal units can be found all over the dendrimer interior. We observe enhanced back-folding towards the dendrimer center for dendrimers with generations $g\geqslant 5$. If the surface region is defined by the condition that the percentage of terminal units has to exceed $n_e(r)/n(r)\geqslant 0.7$ only 10% to 17% of the terminal units are located at the dendrimer surface. However, if we define the surface by the onset of the decay of the density profile at $r\approx R_g$ for high-generation dendrimers, still about 50% of the end groups are located in the dendrimer interior.

No power scaling of the dendrimer radii of gyration with the total number of monomers has been found. In fact the dependency can be well described for all generations by the relation $R_g\propto N^{(2\nu-1)}g^{(1-\nu)}$ suggested by Chen and Cui[25] with $\nu=0.588$, the Flory exponent for good solvent conditions obtained from perturbation calculations for the excluded volume effect.[58] Hence, we would like to conclude that dendrimers do not grow in a self-similar manner when a new generation is added. The dendrimer dimensions change from being closer to those of analogous linear chains for low-generation dendrimers to being closer to those of homogeneous spheres for high generations. In contrast to the behavior of the radii of gyration of the overall dendrimers, the mean center-to-end-bead distances follow rather well a scaling relation close to $R_e\propto N^{0.22}$ for generations $g\geqslant 3$.

Following the evaluation of Mansfield[13] we fitted the initial decay of the pair correlation functions by a power-law decay $\gamma(r)\propto r^{-(3-D)}$, where D can be assigned to the fractal

TABLE III. Generation dependent fractalities D_{sim} and D_{exp} of the dendrimers obtained from a power-law fit $\gamma(r)\propto r^{-(3-D)}$ to the simulated and experimentally determined pair correlation functions $\gamma(r)$, respectively. For comparison simulation results, D_{ref} of Mansfield (Ref. 13) are also shown.

g	D_{exp}	D_{sim}	D_{ref}
0		0.7 ±0.2	0.94
1		1.4 ±0.1	1.64
2	1.84 ±0.01	1.83±0.06	1.99
3	2.000±0.004	2.11±0.04	2.22
4	2.115±0.004	2.32±0.03	2.39
5	2.201±0.005	2.48±0.03	2.51
6	2.351±0.004	2.60±0.02	2.61
7	2.443±0.004	2.71±0.01	2.71
8	2.515±0.003	2.78±0.01	2.79

dimension of the internal dendrimer structure. In agreement with Mansfield's results the fractal dimension is found to vary between approximately $D=5/3\approx 1.67$ as expected for linear chains under good solvent conditions and values close but smaller than 3 as expected for compact objects. However, due to the small dimension of dendrimers the range of length scales where $\gamma(r)$ can be described by a power-law decay is very limited. Even though dendrimers exhibit a fractal topology (architecture), the arrangement in space is not fractal-like and therefore not really manifested in the spatial correlations and size developments.

Finally, we would like to address the question whether our results have a universal character or not. From simulations[53] and experiments[40] on different branching topologies we consider our results as general for rather flexible, star-burst dendrimers. For different core functionalities a shift in generation but no significant change of the results is observed. However, longer spacer between the branching point lead to much looser (starlike) structures with substantially reduced polymer densities in the center. In dendrimers, built from more bulky monomeric units[25] and/or with more bulky end groups,[26,27] back-folding might be suppressed leading to (significant) changes in the mass distributions (cavities) and size developments with increasing generation.

[1] *Dendrimers and Other Dendritic Polymers*, Wiley Series in Polymer Science, edited by J. M. J. Frechet and D. A. Tomalia (Wiley, West Sussex, 2001).
[2] T. J. Prosa, B. J. Bauer, and E. J. Amis, Macromolecules **34**, 4897 (2001).
[3] F. Mallamace, E. Canetta, D. Lombardo, A. Mazzaglia, A. Romeo, L. M. Scolaro, and G. Maino, Physica A **304**, 235 (2002).
[4] R. Kleppinger, H. Reynaers, K. Desmedt, B. Forier, W. Dehaen, M. Koch, and P. Verhaert, Macromol. Rapid Commun. **19**, 111 (1998).
[5] G. Evmenenko, B. J. Bauer, R. Kleppinger, B. Forier, W. Dehaen, E. J. Amis, N. Mischenko, and H. Reynaers, Macromol. Chem. Phys. **202**, 891 (2001).
[6] R. Scherrenberg, B. Coussens, P. van Vliet, G. Edouard, J. Brackman, and E. de Brabander, Macromolecules **31**, 456 (1998).
[7] S. Rosenfeldt, N. Dingenouts, M. Ballauff, N. Werner, F. Vögtle, and P. Lindner, Macromolecules **35**, 8098 (2002).
[8] D. Pötschke, M. Ballauff, P. Lindner, M. Fischer, and F. Vögtle, J. Appl. Crystallogr. **33**, 605 (2000).
[9] A. I. Kuklin, G. M. Ignat'eva, L. A. Ozeriina *et al.*, Polym. Sci., Ser. A Ser. B **12**, 1273 (2002).
[10] S. Rathgeber, M. Monkenbusch, M. Kreitschmann, V. Urban, and A. Brulet, J. Chem. Phys. **117**, 4047 (2002).
[11] A. Topp, B. J. Bauer, J. W. Klimash, R. Spindler, D. A. Tomalia, and E. J. Amis, Macromolecules **32**, 7226 (1999).
[12] T. J. Prosa, B. J. Bauer, E. J. Amis, D. A. Tomalia, and R. Scherrenberg, J. Polym. Sci. A **35**, 2913 (1997).
[13] M. L. Mansfield, Macromolecules **33**, 8043 (2000).
[14] M. L. Mansfield and L. I. Klushin, Macromolecules **26**, 4262 (1993).
[15] K. Karatasos, D. B. Adolf, and G. R. Davies, J. Chem. Phys. **115**, 5310 (2001).
[16] G. Giŭpponi and D. M. A. Buzza, Macromolecules **35**, 9799 (2002).
[17] E. G. Timoshenko, Y. A. Kuznetsov, and R. Connolly, J. Chem. Phys. **117**, 9050 (2002).
[18] E. J. Wallace, D. M. A. Buzza, and D. J. Read, Macromolecules **34**, 7146 (2001).
[19] H. M. Harreis, C. N. Likos, and M. Ballauff, J. Chem. Phys. **118**, 1979 (2003).
[20] R. L. Lescanec and M. Muthukumar, Macromolecules **23**, 2280 (1990).
[21] M. Murat and G. S. Grest, Macromolecules **29**, 1278 (1996).
[22] A. V. Lyulin, G. R. Davies, and D. B. Adolf, Macromolecules **33**, 6899 (2000).
[23] A. V. Lyulin, G. R. Davies, and D. B. Adolf, Macromolecules **33**, 3294 (2000).
[24] L. Lue, Macromolecules **33**, 2266 (2000).
[25] Z. Y. Chen and S.-M. Cui, Macromolecules **29**, 7943 (1996).
[26] L. Cavallo and F. Fraternali, Chem.-Eur. J. **4**, 927 (1998).
[27] M. A. Mazo, N. S. Perov, E. B. Gusarova, P. A. Zhilin, and N. K. Balabaev, Russ. J. Phys. Chem. **74**, S52 (2000).
[28] I. Lee, B. D. Athey, A. W. Wetzel, W. Meixner, and J. R. Baker, Jr., Macromolecules **35**, 4510 (2002). (Mass distribution instead of density profiles are discussed and therefore not compared in detail to results of other authors.)
[29] Y.-J. Sheng, S. Jiang, and H.-K. Tsao, Macromolecules **35**, 7865 (2002).
[30] D. A. Tomalia, A. Naylor, and W. Goddard, Angew. Chem., Int. Ed. Engl. **28**, 138 (1990).
[31] O. J. Glatter, J. Appl. Crystallogr. **10**, 415 (1977).
[32] O. Glatter, J. Appl. Crystallogr. **14**, 101 (1981).
[33] J. S. Pederson and P. Schurtenberger, J. Appl. Crystallogr. **29**, 646 (1996).
[34] B. Loppinet, E. Stiakakis, D. Vlassopoulos, G. Fytas, and J. Roovers, Macromolecules **34**, 8216 (2001).
[35] L. Willner, A. Poppe, J. Allgaier, M. Monkenbusch, P. Lindner, and D. Richter, Macromolecules **30**, 1053 (1997).
[36] L. Willner, O. Jucknischke, D. Richter *et al.*, Macromolecules **27**, 3821 (1994).
[37] W. D. Dozier, J. S. Huang, and L. J. Fetters, Macromolecules **24**, 2810 (1991).
[38] A. Ramzi, M. Prager, D. Richter, V. Efstratiadis, N. Hadjichristidis, R. N. Young, and J. B. Allgaier, Macromolecules **30**, 7171 (1997).
[39] L. Willner, A. Poppe, J. Allgaier, M. Monkenbusch, P. Lindner, and D. Richter, Europhys. Lett. **51**, 628 (2000).
[40] S. Rathgeber, A. P. Gast, and J. L. Hedrick, J. Appl. Phys. A **74**, S396 (2002).
[41] G. Beaucage, J. Appl. Crystallogr. **28**, 717 (1995).
[42] T. Pakula, in *Simulation Methods for Polymers*, *Simulation on the Completely Occupied Lattice in Simulation Methods for Polymers*, edited by M. J. Kotelyanskii and D. N. Theodorou (Dekker, New York, 2004).
[43] T. Pakula and K. Jeszka, Macromolecules **32**, 6821 (1999).
[44] A. Gauger and T. Pakula, Macromolecules **28**, 1900 (1995).
[45] T. Pakula, Comput. Theor. Polym. Sci. **8**, 21 (1998).
[46] T. Pakula, J. Chem. Phys. **95**, 4685 (1991).
[47] D. Boris and M. Rubinstein, Macromolecules **29**, 7251 (1996).
[48] R. La Ferla, J. Chem. Phys. **106**, 688 (1997).
[49] B. Hammouda, J. Polym. Sci. A **30**, 1387 (1992).
[50] W. Burchard, J. Polym. Sci. A **20**, 157 (1982).
[51] P. G. De Gennes and H. L. Hervet, J. Phys. (France) Lett. **44**, L351 (1983).
[52] T. C. Zook and G. T. Pickett, Phys. Rev. Lett. **90**, 015502 (2003).
[53] T. Pakula (unpublished).
[54] B. H. Zimm and W. H. Stockmayer, J. Chem. Phys. **17**, 1301 (1949).
[55] S. Stechemesser and W. Eimer, Macromolecules **30**, 2204 (1997).
[56] W. Carl, J. Chem. Soc., Faraday Trans. **92**, 4151 (1996).
[57] F. Ganazzoli, R. La Ferla, and G. Terragni, Macromolecules **33**, 6611 (2000).
[58] M. Doi and S. F. Edwards, *The Theory of Polymer Dynamics* (Clarendon, Oxford, 1986).